Advanced Photon Source (APS) for their support with x-ray diffraction measurements. We acknowledge the Gordon and Betty Moore Foundation, the Beckman Institute, and the Sanofi-Aventis Bioengineering Research Program for their support of the Molecular Observatory at the California Institute of Technology (Caltech). The operations at the SSRL and APS are supported by the U.S. Department of Energy and the National Institutes of Health (NIH). GM/CA has been funded in whole or in part with federal funds from the National Cancer Institute (ACB-12002) and the National Institute of General Medical Sciences (AGM-12006). T.S. was supported by a Postdoctoral Fellowship of the Deutsche Forschungsgemeinschaft. D.H.L. was supported by a NIH Research Service Award (5 T32 GM07616). A.A.K. was supported by NIH awards U01 GM094588 and U54 GM087519 and by Searle Funds at The Chicago Community Trust. A.H. was supported by Caltech startup funds, the Albert Wyrick V Scholar Award of the V Foundation for Cancer Research, the 54th Mallinckrodt Scholar Award of the Edward Mallinckrodt Jr. Foundation, and a Kimmel Scholar Award of the Sidney Kimmel Foundation for Cancer Research. The coordinates and structure factors have been deposited with the Protein Data Bank with accession codes 4XMM and 4XMN. The authors declare no financial conflicts of interest.

SUPPLEMENTARY MATERIALS

www.sciencemag.org/content/347/6226/1148/suppl/DC1
Materials and Methods
Figs. S1 to S13
Tables S1 and S2
References (*18*–*28*)
Movies S1 to S4

18 September 2014; accepted 27 January 2015
Published online 12 February 2015;
10.1126/science.aaa4136

PROTEIN TARGETING

Structure of the Get3 targeting factor in complex with its membrane protein cargo

Agnieszka Mateja,[1] Marcin Paduch,[1] Hsin-Yang Chang,[1] Anna Szydlowska,[1] Anthony A. Kossiakoff,[1] Ramanujan S. Hegde,[2]* Robert J. Keenan[1]*

Tail-anchored (TA) proteins are a physiologically important class of membrane proteins targeted to the endoplasmic reticulum by the conserved guided-entry of TA proteins (GET) pathway. During transit, their hydrophobic transmembrane domains (TMDs) are chaperoned by the cytosolic targeting factor Get3, but the molecular nature of the functional Get3-TA protein targeting complex remains unknown. We reconstituted the physiologic assembly pathway for a functional targeting complex and showed that it comprises a TA protein bound to a Get3 homodimer. Crystal structures of Get3 bound to different TA proteins showed an α-helical TMD occupying a hydrophobic groove that spans the Get3 homodimer. Our data elucidate the mechanism of TA protein recognition and shielding by Get3 and suggest general principles of hydrophobic domain chaperoning by cellular targeting factors.

Integral membrane proteins contain hydrophobic transmembrane domains (TMDs) that must be shielded from the cytosol until their insertion into the lipid bilayer. Whereas most eukaryotic membrane proteins are cotranslationally targeted to the endoplasmic reticulum (ER) by the signal recognition particle (SRP) (*1*), tail-anchored (TA) membrane proteins are posttranslationally targeted by the cytosolic factor Get3 (*2*–*7*). This conserved adenosine triphosphatase (ATPase) changes conformation in a nucleotide-regulated manner (*8*–*12*) to bind TMDs in the cytosol and release them at its ER membrane receptor (*6*, *13*–*16*).

Assembly of the Get3-TA targeting complex requires "pretargeting" factors that mediate loading onto Get3 (*17*, *18*). This pathway begins with TA protein in complex with the chaperone Sgt2. The Get4-Get5 scaffolding complex then recruits Sgt2 via Get5, while Get4 recruits ATP-bound Get3 (*19*). A hand-off reaction within this complex results in transfer of TA protein from Sgt2 to Get3. TA substrate-loaded Get3 then dissociates from Get4 (*20*–*22*), resulting in a targeting complex whose architecture and stoichiometry have been debated (*8*–*12*, *20*–*23*).

To define the physiologically relevant Get3 targeting complex, we recapitulated its assembly in vitro, using purified recombinant factors at in vivo concentrations (Fig. 1A). Translation of radiolabeled TA protein in the presence of SGTA (the mammalian homolog of Sgt2) produced a stable complex detectable by chemical cross-linking (fig. S1). The TA protein remained associated with SGTA upon addition of either Get4-Get5 or Get3, but released efficiently when both factors were added (Fig. 1B). Correspondingly, Get3 efficiently acquired substrate from SGTA only when Get4-Get5 was present.

The transfer reaction was rapid and unidirectional: Once substrate released from SGTA, it did not rebind (fig. S2). Likewise, substrate preloaded directly on Get3 (fig. S3) did not effectively transfer to SGTA (Fig. 1B). Structure-guided mutations disrupting either the SGTA-Get5 interaction [SGTA(C38S)] (*24*) or the Get4-Get3 interaction [Get3(E253R)] (*20*) abolished substrate release from SGTA (Fig. 1C). Targeting complex produced via Get4-Get5 supported TA protein insertion into yeast ER microsomes (Fig. 1D), while an identical reaction containing SGTA(C38S) showed reduced insertion (Fig. 1D). Thus, the recombinant assembly system requires all factors and interactions of the early GET pathway and produces insertion-competent Get3-TA protein targeting complex.

Three lines of evidence suggested that functional targeting complex assembled via pretargeting factors consists of dimeric Get3 bound to TA protein. First, the targeting complex, containing a small (~10 kD) TA protein, had the same native size as purified Get3 dimer, and was clearly distinguishable from higher-order Get3 complexes (Fig. 1E). Such higher-order complexes, often seen when Get3 is coexpressed with TA protein in *Escherichia coli* (fig. S5) (*8*, *22*, *23*), were not observed even when the loading reaction contained 10-fold excess Get3 (fig. S4A). Second, titration of Get3 into the loading reaction showed no evidence of cooperativity (fig. S4B), arguing against its higher-order assembly during targeting complex formation. Third, size-exclusion chromatography and multiangle laser light scattering (SEC-MALLS) indicated that prior to loading, a single Get3 dimer is bound by two copies of the Get4-Get5 complex (fig S4C). Thus, TA protein is loaded onto dimeric Get3 to form a functional targeting complex.

To gain insight into how the TA protein is shielded by Get3 in this targeting complex, we sought to determine its structure. During physiologic targeting complex assembly, Get4 preferentially recruits and stabilizes adenosine 5′-triphosphate (ATP)–bound Get3 (*19*, *20*, *22*). To mimic this during recombinant expression in *E. coli*, we biased Get3 to the ATP-bound state via the D57N hydrolysis mutant (*10*). Coexpression of this mutant with TA protein resulted in a targeting complex that was homogeneously dimeric for Get3 by SEC-MALLS (fig. S6A) and comigrated with in vitro–assembled targeting complex on sucrose gradients (fig. S6B).

To facilitate crystallization, we generated a high-affinity synthetic antibody fragment (sAB) (*25*) that recognizes the closed (ATP-bound) conformation of Get3. Kinetic analysis revealed that this sAB binds with subnanomolar affinity to nucleotide-bound Get3, both in the presence and absence of TA protein (fig. S7). Thus, rather than inducing a large conformational change in Get3, the TA protein binds to a preorganized conformation that closely resembles the closed (ATP-bound) state.

Using this sAB, we crystallized Get3(D57N) in complex with the TMD of the yeast TA protein

[1]Department of Biochemistry and Molecular Biology, The University of Chicago, 929 East 57th Street, Chicago, IL 60637, USA. [2]MRC Laboratory of Molecular Biology, Francis Crick Avenue, Cambridge CB2 0QH, UK.
*Corresponding author. E-mail: rhegde@mrc-lmb.cam.ac.uk (R.S.H.); bkeenan@uchicago.edu (R.J.K.)

Pep12 (table S1). The structure reveals nucleotide-bound Get3 in a closed conformation with two sABs bound to equivalent sites on opposite faces of a Get3 homodimer (Fig. 2A); no higher-order Get3 oligomers are observed in the crystal (fig. S8). The closed conformation is nearly identical to that seen in previous Get3-ADP•AlF_4^- structures (~0.5 Å root mean square deviation), in which two helical subdomains form a composite hydrophobic groove proposed to bind the TMDs of TA proteins (*8*, *10*).

As is typical for the fungal Get3 crystal structures, electron density is weakest within these dynamic helical subdomains. Nevertheless, unaccounted helical density was visible within the hydrophobic groove in early unbiased maps (fig. S9). After refinement, we assigned this density to the Pep12 TMD (Fig. 2B and fig. S9), excluding the possibility that it corresponds to flexible regions of Get3 folding into the groove.

The Pep12 TMD binds to Get3 at the bottom of the composite hydrophobic groove (Fig. 2 and fig. S9), where it spans the dimer interface and stabilizes the closed conformation of Get3. The most ordered interactions are found at the ends of the TMD, where bulky hydrophobic side chains of the substrate contact groove residues including M97 (helix 4), L126 (helix 5), M143 and M146 (helix 6), L183, L186 and F190 (helix 7), and L216 and L219 (helix 9) (Fig. 2B). Consistent with their role in TMD binding, substitution of hydrophobic residues along helices 7 and 9 with polar or charged residues abolished Get3's ability to induce TA protein release from SGTA (Fig. 3A).

The Pep12 TMD buries ~1450 $Å^2$ of hydrophobic surface area, distributed nearly evenly between the two Get3 subunits (Fig. 2C). This represents ~50% of the ordered hydrophobic surface area in the groove and is significantly greater than in the SRP54-signal peptide interaction, where ~360 $Å^2$ of hydrophobic surface area become buried upon binding (*26*, *27*). The availability of such a large surface area likely explains how Get3 can accommodate hydrophobic sequences of differing lengths and composition.

Using the same strategies, we also solved crystal structures of Get3(D57N) in complex with unrelated TMDs from Nyv1 and Sec22 (table S1). Density for these TMDs was less defined than for the Pep12 complex, but nevertheless sufficient to place helical TMDs (fig. S9). Like Pep12, these TMDs bind at the bottom of the hydrophobic groove, spanning the dimer interface (Fig. 3B). Thus, a single helix binding across the Get3 dimer represents the canonical mode of the Get3-TA substrate interaction.

Although much of the Get3 hydrophobic groove and substrate TMD are shielded in the targeting complexes, one surface of the TMD appears solvent exposed. Relative to previous closed Get3 structures, the groove in each substrate-bound complex is constricted at its apex where the ends of helix 7 curve inwards (Fig. 3B). Although the "TRC40-insert," including helix 8, is poorly defined, we found by site-specific photo–cross-linking that this region (and residues in helix 6 and 7) directly contact the TA substrate (Fig. 3C and fig. S10). Thus, helix 8 likely functions as a dynamic "lid," protecting the TMD from aggregation, while still allowing substrate release after recruitment to Get1 (Fig. 3D) (*13*, *14*).

Our biochemical and structural analyses define the functional targeting complex as a Get3 homodimer bound to a single TA protein. Although higher-order Get3 assembly has been postulated to promote ATP hydrolysis (*22*), this appears unnecessary because dimeric targeting complex was functional for TA protein insertion, indicating that it had hydrolyzed its ATP (Fig. 1D). Consistent with this, the catalytic machinery

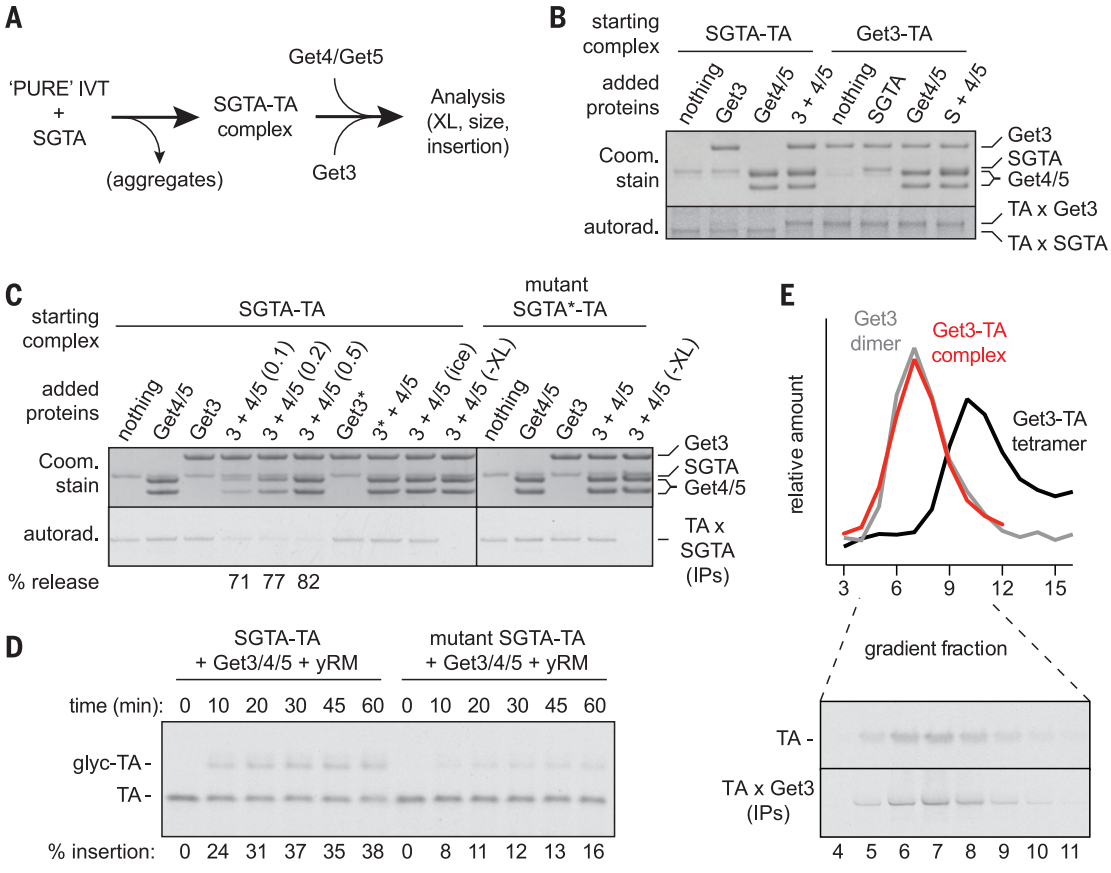

Fig. 1. Reconstitution of physiologic TA protein targeting complex assembly. (**A**) Experimental strategy. (**B**) SGTA-TA or Get3-TA complexes (figs. S1 and S3) at 1 μM were incubated with 1 μM of the indicated proteins, followed by amine-reactive cross-linking. Reactions were analyzed by SDS–polyacrylamide gel electrophoresis and Coomassie blue staining to detect the input proteins (top) or autoradiography to detect the ^{35}S-labeled TA protein cross-links (bottom). (**C**) Reactions as in (B) were monitored by sulfhydryl-reactive cross-linking for TA protein release from SGTA (bottom). Reactions contained 0.5 μM of each factor, except lanes 4 and 5, which contained Get4-Get5 at 0.1 and 0.2 μM, respectively. Asterisks next to Get3 or SGTA indicate point mutants that disrupt interactions with Get4 or Get5, respectively. (**D**) Products of the indicated transfer reactions were incubated with yeast rough microsomes (yRM) and analyzed for insertion. (**E**) Sucrose gradient size analysis of Get3-TA complex formed by Get4-Get5–dependent loading from SGTA (red). Free, dimeric Get3 (gray) and *E. coli*–produced tetrameric Get3-TA substrate complex (black) are shown for comparison (fig. S5). Peak fractions containing substrate (red) were analyzed directly or after cross-linking and immunoprecipitation for Get3 to specifically detect Get3-TA complexes (bottom panel).

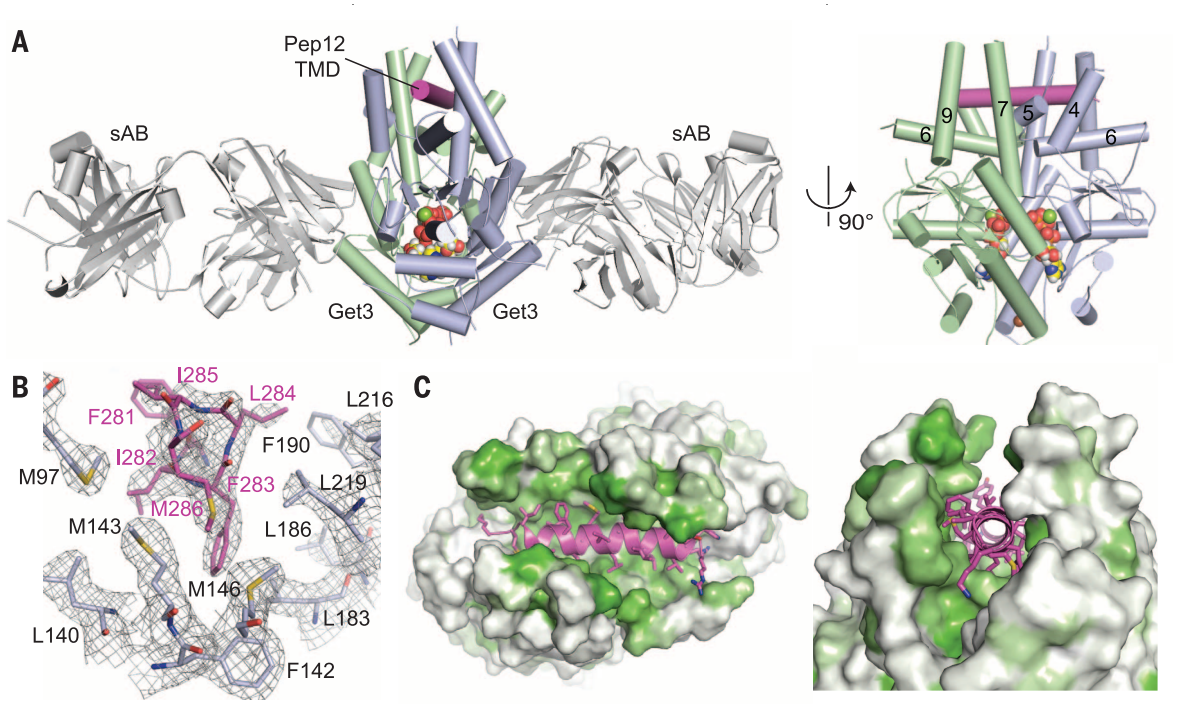

Fig. 2. The helical TMD of a TA substrate binds deep within the composite hydrophobic groove of dimeric Get3. (**A**) Overview of dimeric *Saccharomyces cerevisiae* Get3 bound to a truncated Pep12 TA substrate (magenta) and nucleotide (spheres), and sandwiched between two copies of an engineered sAB (gray). At right, a "side" view of the complex is shown with sABs removed for clarity. (**B**) Details of the interaction between the Pep12 TMD C terminus and a methionine-rich cluster at one end of the hydrophobic groove. Electron density is from a 2.05 Å $2F_o - F_c$ map contoured at 1.0σ. (Amino acid abbreviations: F, Phe; I, Ile; L, Leu; and M, Met.) (**C**) Surface representations of the TA substrate-binding site, colored from least (white) to most (green) hydrophobic.

Fig. 3. Dynamic shielding of the TMD. (**A**) SGTA-TA complexes were prepared and subjected to transfer reactions with wild-type (WT) and mutant Get3 proteins as in Fig. 1C. LL-SS (L183S/L186S), LLL-SSS (L183S/L186S/L219S), and FL-DD (F190D/L216D) are hydrophobic groove mutants; E253R is a mutation that disrupts interaction with Get4. (Amino acid abbreviations: D, Asp; E, Glu; F, Phe; L, Leu; R, Arg; and S, Ser.) (**B**) "Top" and "side" views of Pep12 (magenta), Nyv1 (blue), and Sec22 (green) complexes superimposed on the free Get3 closed dimer structure (yellow; PDB code: 2woj). Relative to free Get3, the end of helix 7 extends and begins to curve inward over the substrate. (**C**) WT or benzophenone-containing (at the indicated positions) Get3-TA complexes were prepared as in fig. S3, and the dimer peak was subjected to ultraviolet (UV) cross-linking. Uncrosslinked TA protein and its adducts to one or two Get3 proteins are indicated. (**D**) "Side" views of the Get3 dimer, looking into the groove. In its transient empty state, Get3 is splayed apart, with two hydrophobic "half-sites" occupied by the helix 8 region. ATP binding drives Get3 into a closed conformation, which is captured by two copies of the Get4-Get5 complex. In this state, helix 8 is displaced, and the composite hydrophobic groove is now preorganized for substrate binding. After substrate transfer from Sgt2, the targeting complex is released. The helix 8 region now dynamically shields the substrate during transit to the ER membrane.

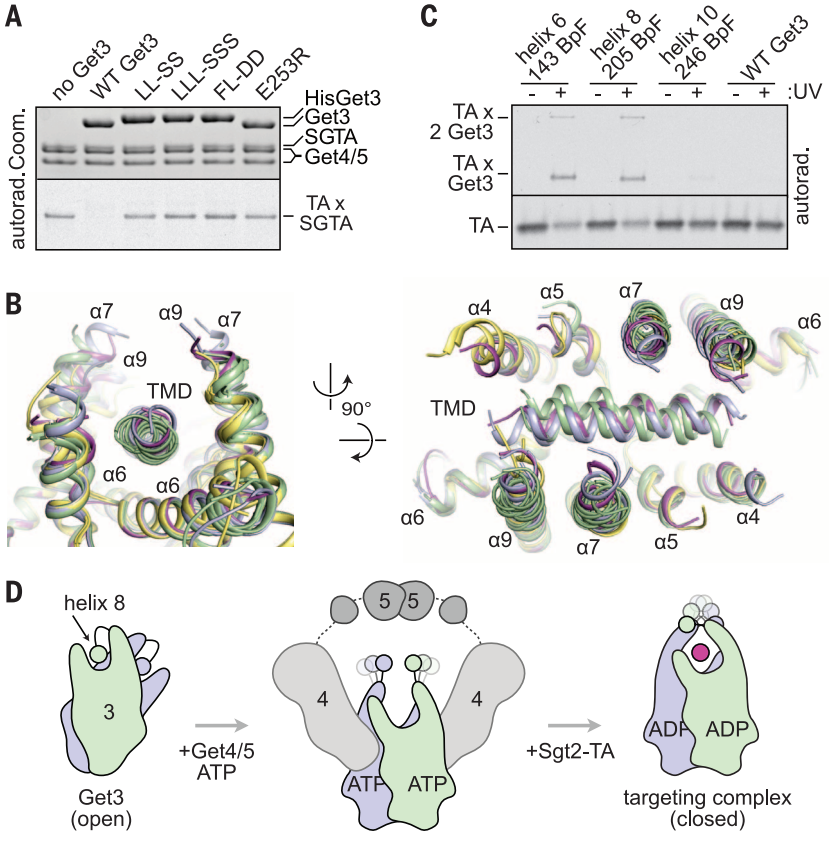

is organized for hydrolysis in the targeting complex structures (fig. S11). The higher-order Get3 oligomers that form during oxidative stress (*28*) are structurally and functionally distinct.

The structure of the Get3-TA substrate targeting complex illustrates a common strategy for binding to hydrophobic cargo. Like Get3, the signal sequence–binding subunit of SRP (SRP54) captures substrates within a hydrophobic, methionine-rich groove presented on a helical scaffold (*26*, *27*, *29*). These scaffolds provide a large and intrinsically dynamic binding site that is not appreciably ordered by substrate capture. This likely confers the ability of Get3 and SRP54 to bind a variety of hydrophobic sequences—an essential property of both targeting systems. It will be of interest to determine whether these principles are shared by other TMD-binding factors, including SGTA and Bag6.

REFERENCES AND NOTES

1. D. Akopian, K. Shen, X. Zhang, S. O. Shan, *Annu. Rev. Biochem.* **82**, 693–721 (2013).
2. J. W. Chartron, W. M. Clemons Jr., C. J. Suloway, *Curr. Opin. Struct. Biol.* **22**, 217–224 (2012).
3. V. Denic, V. Dötsch, I. Sinning, *Cold Spring Harb. Perspect. Biol.* **5**, a013334 (2013).
4. R. S. Hegde, R. J. Keenan, *Nat. Rev. Mol. Cell Biol.* **12**, 787–798 (2011).
5. V. Favaloro, M. Spasic, B. Schwappach, B. Dobberstein, *J. Cell Sci.* **121**, 1832–1840 (2008).
6. M. Schuldiner *et al.*, *Cell* **134**, 634–645 (2008).
7. S. Stefanovic, R. S. Hegde, *Cell* **128**, 1147–1159 (2007).
8. G. Bozkurt *et al.*, *Proc. Natl. Acad. Sci. U.S.A.* **106**, 21131–21136 (2009).
9. J. Hu, J. Li, X. Qian, V. Denic, B. Sha, *PLOS ONE* **4**, e8061 (2009).
10. A. Mateja *et al.*, *Nature* **461**, 361–366 (2009).
11. C. J. Suloway, J. W. Chartron, M. Zaslaver, W. M. Clemons Jr., *Proc. Natl. Acad. Sci. U.S.A.* **106**, 14849–14854 (2009).
12. A. Yamagata *et al.*, *Genes Cells* **15**, 29–41 (2010).
13. S. Stefer *et al.*, *Science* **333**, 758–762 (2011).
14. M. Mariappan *et al.*, *Nature* **477**, 61–66 (2011).
15. F. Wang, C. Chan, N. R. Weir, V. Denic, *Nature* **512**, 441–444 (2014).
16. F. Wang, A. Whynot, M. Tung, V. Denic, *Mol. Cell* **43**, 738–750 (2011).
17. F. Wang, E. C. Brown, G. Mak, J. Zhuang, V. Denic, *Mol. Cell* **40**, 159–171 (2010).
18. M. Mariappan *et al.*, *Nature* **466**, 1120–1124 (2010).
19. J. W. Chartron, C. J. Suloway, M. Zaslaver, W. M. Clemons Jr., *Proc. Natl. Acad. Sci. U.S.A.* **107**, 12127–12132 (2010).
20. H. B. Gristick *et al.*, *Nat. Struct. Mol. Biol.* **21**, 437–442 (2014).
21. M. E. Rome, U. S. Chio, M. Rao, H. Gristick, S. O. Shan, *Proc. Natl. Acad. Sci. U.S.A.* **111**, E4929–E4935 (2014).
22. M. E. Rome, M. Rao, W. M. Clemons, S. O. Shan, *Proc. Natl. Acad. Sci. U.S.A.* **110**, 7666–7671 (2013).
23. C. J. Suloway, M. E. Rome, W. M. Clemons Jr., *EMBO J.* **31**, 707–719 (2012).
24. J. W. Chartron, D. G. VanderVelde, W. M. Clemons Jr., *Cell Reports* **2**, 1620–1632 (2012).
25. M. Paduch *et al.*, *Methods* **60**, 3–14 (2013).
26. T. Hainzl, S. Huang, G. Meriläinen, K. Brännström, A. E. Sauer-Eriksson, *Nat. Struct. Mol. Biol.* **18**, 389–391 (2011).
27. C. Y. Janda *et al.*, *Nature* **465**, 507–510 (2010).
28. W. Voth *et al.*, *Mol. Cell* **56**, 116–127 (2014).
29. R. J. Keenan, D. M. Freymann, P. Walter, R. M. Stroud, *Cell* **94**, 181–191 (1998).

ACKNOWLEDGMENTS

We thank S. Shao for help with assay development; S. Koide for the phage library; S. Sidhu for the sAB expression vector; M. Kivlen for plasmids; F. Bezanilla, E. Perozo ,and J. Piccirilli for instrumentation; members of the Keenan, Hegde, and Kossiakoff labs for support; and the NE-CAT (24-ID-C) beamline staff at Advanced Photon Source for technical assistance. NE-CAT is supported by NIH grant P41 GM103403 and U.S. Department of Energy contract DE-AC02-06CH11357. Additional support was from the UK Medical Research Council (MC_UP_A022_1007 to R.S.H.), the NIH (U01 GM094588 and U54 GM087519 to A.A.K.; R01 GM086487 to R.J.K.), and the Searle Funds at The Chicago Community Trust for the Chicago Biomedical Consortium (to A.A.K. and R.J.K.). The Protein Data Bank (PDB) accession codes are 4XTR (Pep12), 4XVU (Nyv1), and 4XWO (Sec22).

SUPPLEMENTARY MATERIALS

www.sciencemag.org/content/347/6226/1152/suppl/DC1
Materials and Methods
Supplementary Text
Figs. S1 to S12
Table S1
References (*30*–*37*)

23 September 2014; accepted 30 January 2015
10.1126/science.1261671

EVOLUTIONARY GENOMICS

Evolutionary changes in promoter and enhancer activity during human corticogenesis

Steven K. Reilly,[1]* Jun Yin,[1]* Albert E. Ayoub,[2,3] Deena Emera,[1] Jing Leng,[1,4]† Justin Cotney,[1] Richard Sarro,[1] Pasko Rakic,[2,3] James P. Noonan[1,2,4]‡

Human higher cognition is attributed to the evolutionary expansion and elaboration of the human cerebral cortex. However, the genetic mechanisms contributing to these developmental changes are poorly understood. We used comparative epigenetic profiling of human, rhesus macaque, and mouse corticogenesis to identify promoters and enhancers that have gained activity in humans. These gains are significantly enriched in modules of coexpressed genes in the cortex that function in neuronal proliferation, migration, and cortical-map organization. Gain-enriched modules also showed correlated gene expression patterns and similar transcription factor binding site enrichments in promoters and enhancers, suggesting that they are connected by common regulatory mechanisms. Our results reveal coordinated patterns of potential regulatory changes associated with conserved developmental processes during corticogenesis, providing insight into human cortical evolution.

The massive expansion and functional elaboration of the neocortex underlies the advanced cognitive abilities of humans (*1*). Although the overall process of corticogenesis is broadly conserved across mammals, humans exhibit differences that emerge within the first 12 weeks of gestation. Among these are an increased duration of neurogenesis, increases in the number and diversity of progenitors, modification of neuronal migration, and introduction of new connections among functional areas (*2*, *3*). The genetic changes responsible for these evolutionary novelties are largely unknown.

Changes in gene regulation are hypothesized to be a major source of evolutionary innovation during development (*1*, *3*, *4*). Critical events in corticogenesis, including the specification of cortical areas and differentiation of cortical layers, rely on the precise control of gene expression (*4*). The evolution of distinctly human cortical features required changes in many of these early developmental processes, which may have been driven by modifications in the gene regulatory programs that govern them. However, identifying such regulatory changes and linking them to relevant biological processes has proven to be challenging. Previous efforts have relied on comparative genomics or on gene expression comparisons at later developmental and adult stages (*5*–*7*). Further progress has been hindered by the lack of genome-wide maps of regulatory function during corticogenesis.

Genome-wide profiling of posttranslational histone modifications associated with regulatory functions has been used to compare regulatory element activities across species (*8*–*12*). In this work, we profiled H3K27ac and H3K4me2 to map active promoters and enhancers during human, rhesus macaque, and mouse corticogenesis, as well as to identify increases in their activity in humans. We examined biological replicates of whole human cortex at 7 postconception weeks (p.c.w.) and 8.5 p.c.w. and primitive frontal and occipital tissues from 12 p.c.w. (Fig. 1A). These stages span the appearance of the transient embryonic zones that generate cortical neurons from the deep to the superficial layers, when distinctly human features of the cortex begin to emerge

[1]Department of Genetics, Yale School of Medicine, New Haven, CT 06510, USA. [2]Kavli Institute for Neuroscience, Yale School of Medicine, New Haven, CT 06510, USA. [3]Department of Neurobiology, Yale School of Medicine, New Haven, CT 06510, USA. [4]Program in Computational Biology and Bioinformatics, Yale University, New Haven, CT 06511, USA.
*These authors contributed equally to this work. †Present address: Illumina, 499 Illinois Street, San Francisco, CA 94158, USA.
‡Corresponding author. E-mail: james.noonan@yale.edu

www.sciencemag.org/content/347/6226/1152/suppl/DC1

Supplementary Materials for

Structure of the Get3 targeting factor in complex with its membrane protein cargo

Agnieszka Mateja, Marcin Paduch, Hsin-Yang Chang, Anna Szydlowska, Anthony A. Kossiakoff, Ramanujan S. Hegde,* Robert J. Keenan*

*Corresponding author. E-mail: rhegde@mrc-lmb.cam.ac.uk (R.S.H.); bkeenan@uchicago.edu (R.J.K.)

Published 6 March 2015, *Science* **347**, 1152 (2015)
DOI: 10.1126/science.1261671

This PDF file includes:

Materials and Methods:

Preparation of individual proteins for functional analysis

Genes encoding full-length *S. cerevisiae* Get4, Get5 and Sgt2 were PCR amplified from genomic DNA. Sgt2 was subcloned into pET21c (Novagen) in-frame with a C-terminal 6xHis tag; Get5 was subcloned into a pCDF1b derivative (Novagen) modified to incorporate a tobacco etch virus (TEV) protease cleavage site between an N-terminal 6xHis tag and the polylinker; Get4 was subcloned into pET28 (Novagen) without modification. Full-length human SGTA was subcloned into pGEX6p1 with a 3C protease cleavage site between an N-terminal GST tag and the polylinker. Site-directed mutants were obtained by QuikChange mutagenesis (Stratagene) and verified by DNA sequencing.

Expression and purification of full-length Get3 (wild-type and mutants) was carried out as described previously (*10*). For photocrosslinking experiments, wild-type Get3 amber mutants prepared with a C-terminal 6xHis tag, were co-transformed with pEVOL-pBpF (*30*) into *E. coli* BL21(DE3) (Novagen). After the cells reached ~0.6 A_{600}, 0.1 mM IPTG, 0.2% arabinose and 1 mM *p*-benzoylphenylalanine (BpF) (Bachem) were added, and the culture was grown for an additional 6 h at 25 °C. Purification was as above for Get3 except that 50 mM Hepes pH 7.5 was used as the buffer. Dimeric Get3-BpF mutants were purified by gel filtration and then used for photocrosslinking experiments.

Full-length Get4 and Get5 (wild-type and mutants) were co-expressed for 6 h at 25 °C in *E. coli* BL21(DE3)/pRIL, following induction with 0.1 mM IPTG. Cells were disrupted in buffer A (50 mM Tris, 500 mM NaCl, 10 mM imidazole, 5% glycerol, 5 mM β-mercaptoethanol, pH 7.5) with 1 mM PMSF and 0.02 mg/mL DNase using a high-pressure microfluidizer (Avestin). After clearing by centrifugation, the supernatant was batch-purified by nickel-affinity chromatography. Protein was eluted in buffer A containing 200 mM imidazole, and then dialyzed into 20 mM Tris, 200 mM NaCl, 2 mM DTT, pH 7.5. This was typically followed by gel filtration (Superdex 200 10/300 GL, GE Healthcare) in 20 mM Tris, 200 mM NaCl, 2 mM DTT, pH 7.5. Fractions were pooled and stored in aliquots at -80 °C. Protein concentrations were determined by Bradford (Bio-Rad).

Full-length human SGTA (wild-type and mutants) was expressed for 16 h at 16 °C in *E. coli* BL21(DE3), following induction with 0.2 mM IPTG. The GST-fusion was purified by standard methods and eluted with glutathione, followed by dialysis into 50 mM Hepes 7.4, 150 mM KOAc, 2 mM $MgCl_2$, 1 mM DTT, and 10% Glycerol. After cleavage with 3C protease and subtraction using Glutathione resin, the protein was concentrated using Vivispin 10K cutoff filters and stored in aliquots at -80 °C.

Multi-angle laser light scattering

To obtain protein for size analysis (see fig. S5 and S6), dimeric targeting complexes were produced by co-expression in *E. coli* BL21(DE3)/pRIL (Novagen) after co-transformation with a plasmid encoding Get3(D57N), and a plasmid derived from the PURE system control plasmid (NEB) in which DHFR was replaced with full-length *S. cerevisiae* Sbh2 containing N-terminal Twin-strep and C-terminal opsin tags and a Pep12 TMD. Protein was expressed at RT for 4 h by induction with 0.1 mM IPTG after the cells reached an A_{600} of ~0.8. Cells were disrupted in buffer B (100 mM Tris, 150 mM NaCl, pH 8.0) and cleared by centrifugation. The supernatant was passed over Strep-Tactin agarose (IBA, Germany) three times. After washing with ten column volumes of buffer B, targeting complex was eluted with buffer B supplemented with 5

mM desthiobiotin (Novagen). These complexes were further purified by gel filtration in 10 mM Tris, 150 mM NaCl, pH 7.5. Fractions were pooled, concentrated, and stored in aliquots at -80 °C. Protein concentration was determined by Bradford assay (Bio-Rad).

Tetrameric targeting complexes were obtained similarly, except using wild-type Get3 and a truncated N-terminally 6xHis tagged $Pep12^{262-288}$ substrate subcloned into pET28. Protein was expressed and purified as described below for the Get3(D57N)-TA substrate complexes.

Full-length Get3(D57N)-Get4-Get5 complexes were obtained by incubating Get3(D57N) (containing an N-terminal 6xHis tag) with 2 mM ATP and 2 mM $MgCl_2$. After incubating for 15 minutes, Get4-Get5 (with an N-terminal 6xHis tag on Get5) was added to give final protein concentrations of 60 μM Get3(D57N), and 40 μM Get4-Get5. Samples were incubated for an additional 30 minutes and then analyzed immediately.

The absolute molecular masses of targeting complexes were measured by static multi-angle laser light scattering (MALLS), essentially as described (*14*). Samples were injected onto a Superdex 200 10/300 GL gel-filtration column (GE Healthcare) equilibrated with 20 mM Tris, 150 mM NaCl, pH 7.5 (targeting complexes) or 20 mM Hepes, 150 mM NaCl, 0.5 mM ATP, 0.5 mM MgCl2, pH 7.5 [Get3(D57N)/4/5 and Get4-Get5 complexes]. The purification system was coupled to an online, static, light scattering detector (Dawn HELEOS II, Wyatt Technology), a refractive-index detector (Optilab rEX, Wyatt Technology) and a ultraviolet-light detector (UPC-900, GE Healthcare). Absolute weight-averaged molar masses were calculated using the ASTRA software (Wyatt Technology).

Tail-anchored substrate transfer reaction

A previously described native human Sec61β construct (*7*) was modified to contain the TMD from VAMP, followed by a C-terminal opsin tag (fig. S1). This ORF was subcloned in place of DHFR in the control T7-driven plasmid for in vitro transcription and translation in the PURE system (NEB). Yeast Get3 antibody was as described previously (*10*). The SGTA antibody was generated against a synthetic C-terminal peptide conjugated to KLH. The SGTA sequence used was CRSRRPSASNDDQQE, with the extra cysteine added at the N-terminus for KLH conjugation.

Chaperone-TA complexes were obtained by supplementing the PURE translation system (NEB) with plasmid encoding the VAMP TMD-containing substrate, ^{35}S-methionine and 25 μM of purified Sgt2, SGTA or Get3. After incubating for 90 min at 37 °C, reactions were diluted with ice cold assay buffer (50 mM Hepes pH 7.4, 125 mM KOAc, 2 mM $MgCl_2$), and separated at 4 °C through a 5-25% sucrose gradient (55,000 rpm/5 h in a TLS55 rotor); fractions containing the soluble complexes (see fig. S1 and S3) were pooled and either used immediately or frozen in liquid nitrogen and stored at -80 °C.

Substrate transfer reactions were carried out in 50 mM Hepes pH 7.4, 125 mM KOAc, 4 mM $MgCl_2$ and 1 mM ATP and subjected to amine-reactive, sulfhydryl-reactive, or UV crosslinking. Amine-reactive crosslinking used 250 μM disuccinimidyl suberate (Pierce) at 22° C for 30 min. Sulfhydryl-reactive crosslinking used 200 μM bismaleimidohexane (Pierce) for 30 min on ice. Photo-crosslinking via BpF with UV was for 15 min on ice using a 365 nm longwave UV spot lamp (UVP) placed 10 cm from the sample. All crosslinking reactions were terminated by addition of excess SDS-PAGE buffer, followed optionally by immunoprecipitation (with anti-SGTA or anti-Get3 antibodies), separation by SDS-PAGE on 12% Tris-Tricine gels, Coomassie blue staining and autoradiography.

Size analysis of the Get3-TA substrate complexes formed by Get4-Get5-dependent loading from SGTA was performed using high-resolution 5-25% sucrose gradients (55,000 rpm/5 h in a TLS55 rotor); gradient fractions were analyzed by SDS-PAGE and quantified by phosphorimaging. Free, dimeric Get3 and *E. coli*-produced tetrameric Get3-TA substrate complexes (described above) were used as molecular weight standards; samples were analyzed by Coomassie staining and quantified by densitometry.

Insertion activity was analyzed by incubating TA substrate complexes (as indicated in the Figure legends) with yeast rough microsomes, prepared from wild-type yeast essentially as described previously (*14*). Insertion was monitored by TA protein glycosylation and quantified by phosphorimaging.

Phage display

Gel filtration purified Get3(D57N) (130 μM in 20 mM Hepes, 150 mM NaCl, pH 8.0) was preincubated with 2 mM ATP and 2 mM $MgCl_2$ for 30 minutes, followed by addition of a 5-fold molar excess of biotinylation reagent (NHS-SS-PEG4-Biotin) (Thermo Scientific). Biotinylation was carried out for 1 h at 25 °C and quenched with 2 mM Tris pH 8.0. After desalting on a PD10 column, Get3(D57N) dimers were purified by SEC and concentrated. The extent of biotinylation and efficiency of antigen capture were tested by pulldown with Streptavidin MagneSphere particles. To obtain sABs selective to the closed conformation of Get3, solutions were supplemented with 2 mM ATP and 2 mM $MgCl_2$ throughout the selection process. Phage display (using a synthetic antibody phage library provided by S. Koide) and initial clone testing was performed as described previously (*25*). Conformational specificity was confirmed in single point competitive ELISA prior to gel filtration analysis and kinetic analysis by SPR (see below).

sAB production

sABs were subcloned into the expression vector RH2.2 (gift from S. Sidhu) using Hind III and SalI restriction sites. Sequence confirmed clones were transformed into *E. coli* BL21 (DE3)/pRIL (Novagen) and sABs were expressed for 24 h at 25 °C using autoinduction in a LEX fermentor system with air flow rate of 2 L/min. Cells were disrupted in lysis buffer containing 50 mM Tris, 500 mM NaCl, and 0.05% Triton X-100, pH 8.0 using a high pressure microfluidizer (Avestin). Lysate was cleared by centrifugation and loaded onto HiTrap MabSelect SuRe 5 mL column, equilibrated with buffer containing 50 mM Tris, 500 mM NaCl pH 8.0. Column was washed with 10 volumes of equilibration buffer and then protein was eluted with 0.1 M acetic acid. Fractions containing protein were directly loaded onto ion exchange Resource S 1 mL column. Column was washed with buffer containing 50 mM sodium acetate pH 5.0 at 5 mL/min. sABs were eluted with a linear gradient 0-50% of buffer containing 50 mM sodium acetate, 2 M NaCl, pH 5.0. Pure sABs were dialyzed against buffer containing 20 mM Tris, 150 mM NaCl, pH 7.5.

Surface plasmon resonance

Interaction analyses were performed at 20 °C using a BIACORE 3000 (GE Healthcare). SEC purified, 6xHis tagged Get3(D57N) and Get3(D57N)- $Pep12^{262-288}$ complex (with an N-terminal 6xHis tag on the TA substrate only) were immobilized on an NTA sensor chip. For the analysis, running buffer contained: 10 mM Hepes, 150 mM NaCl, pH 7.4, 0.05% Tween 20 supplemented with 1 mM $MgCl_2$ and +/- 1 mM nucleotide (ATP or ADP). 6xHis-tagged Get3(D57N) and Get3(D57N)- $Pep12^{262-288}$ complex were captured by injecting 5 μL of 30 nM

protein solution at a flow rate of 5 µL/min. Up to three blanks were injected to ensure stability of the surface before analyte injections were started. For each assay, two-fold dilution series of sAB (clone ID 47E1_2) starting at 10 nM were injected over the NTA chip surface at a flow rate of 30 µL/min to minimize mass transport effects for 150 s. The resulting response unit change was measured for 300 s after the injection finished. Following each sample injection, the NTA chip surface was regenerated with 50 µL of 5 M GdmHCl, 100 mM EDTA, 2% Tween 20 solution at a flow rate of 50 µL/min. All conditions were tested at 7 different sAB concentrations, and each concentration was tested in triplicate. Injections were randomized to avoid systematic errors. Data processing and kinetic analysis were performed using in Scrubber 2 program (BioLogic software). All sensorgrams were double referenced using blank channel and buffer injections. For the determination of kinetic rate constants, all data sets were fit to a simple 1:1 interaction model using nonlinear regression analysis.

Preparation of Get3(D57N)-TA substrate complexes for crystallization

The gene encoding native, full-length *S. cerevisiae* Get3(D57N) was subcloned into pCDF1b (Novagen). Truncated TA substrates corresponding to $Pep12^{262-288}$, $Sec22^{184-214}$ and $Nyv1^{225-251}$, modified to contain an N-terminal 6xHis tag, were subcloned into pET28. TA substrate and Get3(D57N) plasmids were co-transformed into *E. coli* BL21(DE3)/pRIL (Novagen), and expression was carried out at room temperature for 6 h following induction with 0.1 mM IPTG after the cells reached an A_{600} of ~0.6. After resuspending in buffer A supplemented with 1 mM PMSF, cells were disrupted using a microfluidizer (Avestin). After clearing by centrifugation, the supernatant was batch-purified by nickel-affinity chromatography. Protein was eluted in buffer A containing 200 mM imidazole, dialyzed into 20 mM Tris, 200 mM NaCl, 2 mM DTT, pH 7.5 and followed by gel filtration (Superdex 200 10/300 GL, GE Healthcare) in 20 mM Tris, 150 mM NaCl, pH 7.5. Fractions corresponding to dimeric Get3(D57N)-TA substrate complex were pooled, concentrated and stored in aliquots at -80 °C. Protein concentrations were determined by Bradford assay (Bio-Rad).

Purified Get3(D57N)-TA substrate complexes were incubated for 30 minutes with 2 mM ATP and 2 mM $MgCl_2$ (Sec22, Nyv1) or with 2 mM ADP and 2 mM $MgCl_2$ (Pep12). Note that to conserve reagents (especially the sAB), we did not prepare all TMD-nucleotide combinations, under the assumption that we would be able to fully exchange nucleotide on the comparatively slow timescale of crystallization. Next, the complex was incubated for 30 min with a 1.2 molar excess of purified sAB (clone ID 47E1_2), and then spun down at 13,000 rpm for 10 minutes at 4 °C. Finally, the complex was separated from excess sAB by gel filtration. Fractions were pooled, concentrated to ~8-10 mg/mL in 10 mM Tris, 150 mM NaCl, pH 7.5, and stored in aliquots at -80 °C.

Crystallization and data collection

All crystals of the *S. cerevisiae* Get3(D57N)-TA complexes with sAB were grown at room temperature by hanging drop vapor diffusion. Initial high-throughput screening was done with either ATP or ADP added in excess to the protein solution. Although we obtained crystals in both nucleotide conditions, the most promising were with ATP for Pep12 and Nyv1, and ADP for Sec22; these were subsequently optimized. Micro-crystals from screening experiments were crushed and used to seed experiments using varying concentrations of PEG 3350 and succinic acid pH 7.0. Optimization led to the production of single crystals.

Crystals of Get3(D57N)-Pep12$^{262-288}$ were obtained by mixing equal volumes of a protein solution containing 2 mM ATP and 2 mM $MgCl_2$ with a reservoir solution containing 16% PEG 3350 and 25 mM succinic acid pH 7.0. Crystals were cryoprotected in mother liquor supplemented with 20% ethylene glycol, 2 mM ATP and 2 mM $MgCl_2$, and flash frozen in liquid nitrogen.

Crystals of the *S. cerevisiae* Get3(D57N)-Nyv1$^{225-251}$ complex with sAB were grown by mixing equal volumes of protein solution containing 2 mM ATP and 2 mM $MgCl_2$ with 15% PEG 3350, 25 mM succinic acid pH 7.0. Crystals were cryoprotected in mother liquor supplemented with 10% PEG 400, 2 mM ATP and 2 mM $MgCl_2$, and flash frozen in liquid nitrogen.

Crystals of the *S. cerevisiae* Get3(D57N)-Sec22$^{184-214}$ complex with sAB were obtained by mixing equal volumes of a protein solution containing 2 mM ADP and 2 mM $MgCl_2$ with a reservoir solution containing 13% PEG 3350, 25 mM succinic acid pH 7.0. Crystals were briefly soaked in mother liquor supplemented with 20% ethylene glycol, 2 mM ADP, and 2 mM $MgCl_2$, and flash frozen in liquid nitrogen.

The presence of all protein components (including the TMD) was established by analyzing washed crystals by SDS-PAGE (fig. S12). All diffraction data were collected from single crystals at 100 K at APS beamline 24ID-C (lambda=0.9795 Å) on a PILATUS 6MF pixel-array detector. Data were processed using the Xia2 (*31*) pipeline to XDS (*32*); data collection and processing statistics are listed in table S1.

Structure determination and refinement

The structure of the Pep12$^{262-288}$ complex was determined to a resolution of 2.05 Å by molecular replacement with PHASER (*33*), using the closed dimer form of *S. cerevisiae* Get3 (PDB 2woj; with the helical subdomain trimmed) (*10*), and a sAB (PDB 3pgf, with the complementarity determining regions omitted) (*34*), used as search models. Unbiased electron density maps, calculated after manual building and refinement of Get3 and the sAB, revealed clear positive *F*o-*F*c difference density for the helical Pep12 TMD (fig. S9). After initial placement of the TMD, iterative refinement and model building in PHENIX (*35*) and COOT (*36*) allowed us to assign its sequence (Fig. 2). The final model contains one Get3 homodimer, one Pep12 TMD, two sAB complexes, one zinc atom, two magnesium atoms, two molecules each of ADP and ATP (with average occupancies of 0.36 and 0.64 respectively) and 928 water molecules.

The structures of the Nyv1$^{225-251}$ (determined to 2.35 Å) and Sec22$^{184-214}$ (determined to 2.75 Å) complexes were obtained by molecular replacement as described above, except that the refined model for the sAB (from the Pep12 complex) was used along with trimmed 2woj dimer as the search models. Weak difference density was visible within the groove in unbiased electron density maps (fig. S9). After placement of a helical TMD, additional refinement and model building confirmed the presence of the TMDs; however, because the density was weak, we modeled the TMDs as poly-alanine helices and did not define their orientation. The final Nyv1 model contains two Get3 homodimers, two Nyv1 TMDs, four sAB complexes, two zinc atoms, four magnesium atoms, four ATP molecules and 808 waters; The final Sec22 model contains four Get3 homodimers, four Sec22 TMDs, eight sAB complexes, four zinc atoms, eight magnesium atoms, eight molecules each of ADP and ATP (with average occupancies of 0.45 and 0.55 respectively), and 425 waters.

Refinement and validation statistics are listed in table S1. Structure figures were generated using PyMOL (http://www.pymol.org/).

Over the course of this project we screened the diffraction properties of hundreds of crystals and collected a series of datasets on different Pep12, Nyv1 and Sec22 crystals; these diffracted to varying resolutions, and often possessed different space groups and cell dimensions. The best of these datasets gave rise to electron density maps that showed convincing helical TMD density in the hydrophobic groove; others, while largely identical in structure, were apparently less ordered in the groove, making assignment of the TA substrate difficult. However, there was no obvious correlation between nucleotide state and the quality of electron density in the groove. Importantly, the Nyv1 complex (space group *P*1; ATP only), Pep12 (space group $P2_12_12_1$; mixture of ATP/ADP) and Sec22 (space group *P*1; mixture of ATP/ADP) are remarkably similar—both in terms of overall structure and in the active site details (see fig. S11), despite the different crystal forms and nucleotide composition. Thus, the structures we report do not appear to be sensitive to ATP vs. ADP.

Supplementary Text

Author contributions

A.M. and R.S.H. carried out the biochemical and functional studies; A.M. and M.P. performed the sAB selection and subsequent characterization with guidance from A.A.K.; H-Y.C. and A.S. contributed at the early stages of the project to characterize the *E. coli* produced targeting complexes; A.M. carried out the crystallization and data collection, and with R.J.K., solved and analyzed the structures.; R.J.K. conceived the project and guided experiments; R.S.H. and R.J.K. wrote the manuscript with input from all authors.

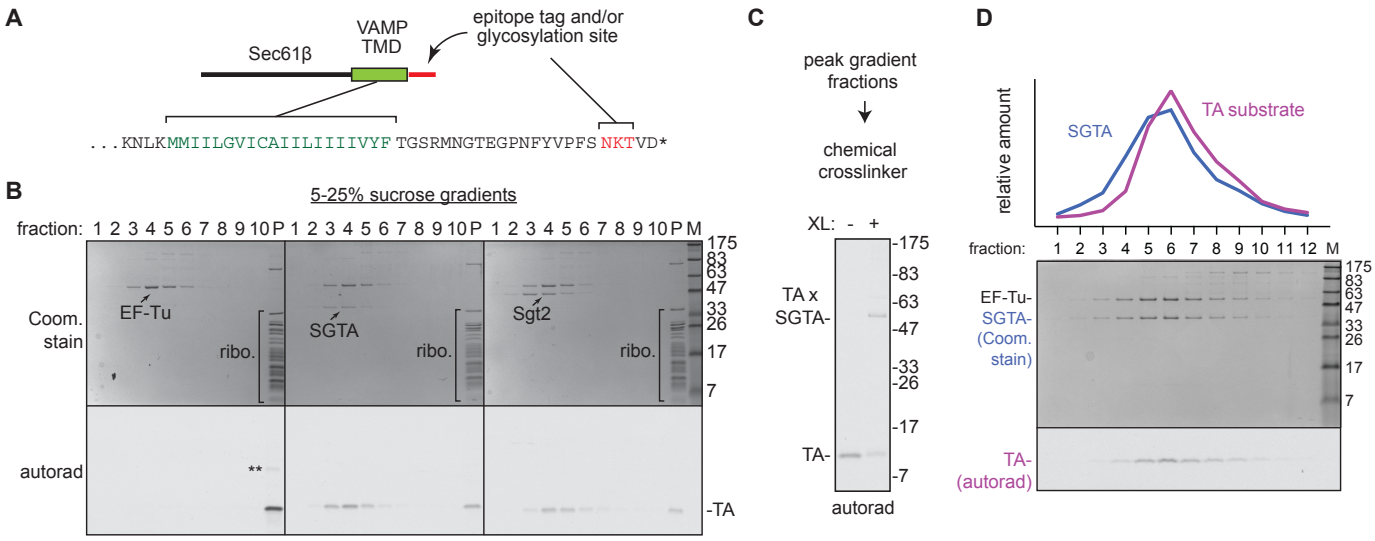

Fig. S1. Formation of chaperone-client complexes by *E. coli* PURE translation.

(A) Schematic of the model TA protein used for functional analyses. Native human Sec61β (*7*) was modified to contain the highly hydrophobic TMD from VAMP (green) followed by the Opsin tag (red) containing a consensus site for N-glycosylation. The VAMP TMD-containing construct (*18*) and the Opsin tag (*37*) have been characterized. **(B)** Plasmid encoding the model TA protein (from panel A) was used to program the PURE translation system containing ^{35}S-methionine. The reaction either lacked (left) or contained (other two panels) recombinant SGTA or Sgt2 at 25 μM. Reaction products were separated on a 5-25% sucrose gradient and analyzed by SDS-PAGE, Coomassie blue staining (top panels), and autoradiography (bottom panels). The ribosomes, which sediment to the bottom of the gradient, and EF-Tu (an abundant component of the PURE system visible by Coomassie staining) are indicated. The ^{35}S-labeled TA protein sediments to the bottom of the gradient (presumably as aggregates) in the absence of any chaperone. This sample also contains SDS-resistant dimers (asterisks) and higher order aggregates visible as a faint smear of increased molecular weight. Including a chaperone in the reaction substantially reduces aggregation of the TA protein, which now co-migrates with the chaperone in fractions 3-5. Note that both Sgt2 and SGTA form complexes with the TA protein with comparable efficiency. **(C)** SGTA-TA protein complex formed as in panel B was treated with the sulfhydryl-reactive crosslinker BMH and analyzed by SDS-PAGE. Highly efficient crosslinking between TA protein and SGTA was observed (and confirmed by anti-SGTA immunoprecipitation; data not shown). Similar crosslinking was seen with the amine-reactive crosslinker DSS, albeit with reduced efficiency. Sgt2-containing complexes did not crosslink with BMH, presumably due to its single cysteine being inaccessible. Sgt2 crosslinking could be seen with DSS, but again, was relatively inefficient, and due to numerous surface lysine residues, rather heterogeneous (data not shown). **(D)** Analysis of SGTA-TA complex on a higher resolution 5-25% sucrose gradient shows the co-migration of the chaperone (blue) and TA protein (purple) as a symmetric peak. Comparison to free chaperone (which is a homodimer as judged by SEC-MALLS; not shown) indicates that the SGTA-TA complex is essentially identical in size, suggesting that the TA protein (~10 kDa) forms a complex with an SGTA dimer.

Thus, the chaperones SGTA or Sgt2 can interact with and form soluble complexes with a TA protein produced in a defined heterologous translation system. For several technical reasons, we used SGTA complexes for our subsequent functional assays. First, the interaction with and release of TA protein could be efficiently and cleanly assayed by crosslinking. Second, we have antibodies to SGTA that work efficiently by IP. Third, SGTA is several kDa smaller than Get3, making it possible to separate their respective crosslinked products by SDS-PAGE. Since the key interaction regions between Sgt2-Get5 and SGTA-Ubl4A are highly conserved, its compatibility with the yeast factors was likely (as borne out by subsequent experiments). Furthermore, functional studies in the mammalian system (Shao et al., in preparation) verified that SGTA is the mammalian functional homolog of Sgt2.

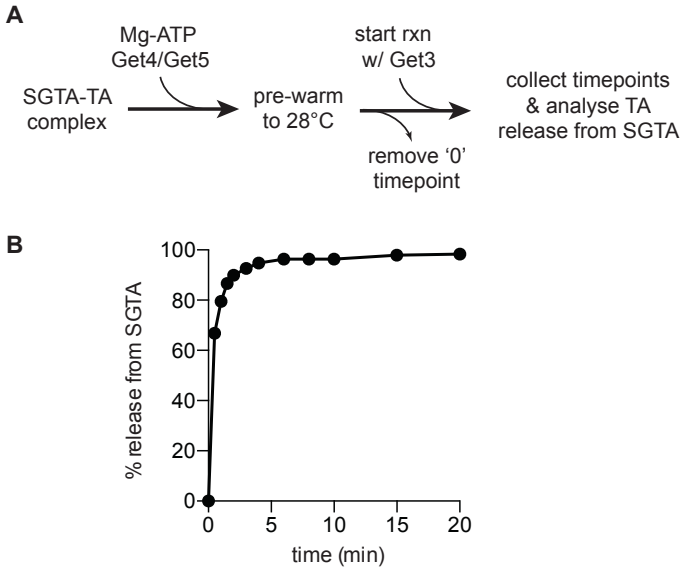

Fig. S2. Time course of TA protein transfer from SGTA to Get3.

(A) Schematic showing the experimental setup in which SGTA-TA complexes (at 0.5 μM) are mixed with Get4-Get5 (0.5 μM) and Mg-ATP (1 mM), pre-warmed briefly to the reaction temperature of 28°C, and supplemented with Get3 (0.5 μM) to initiate the reaction. The transfer reaction was assayed by monitoring the disappearance of SGTA-TA crosslinks (quantified by phosphorimaging), an event entirely dependent on both Get4-Get5 and Get3 (as shown in Fig. 1). **(B)** Time course of transfer as monitored by TA protein release from SGTA ($t_{½}$ ~ 30 sec).

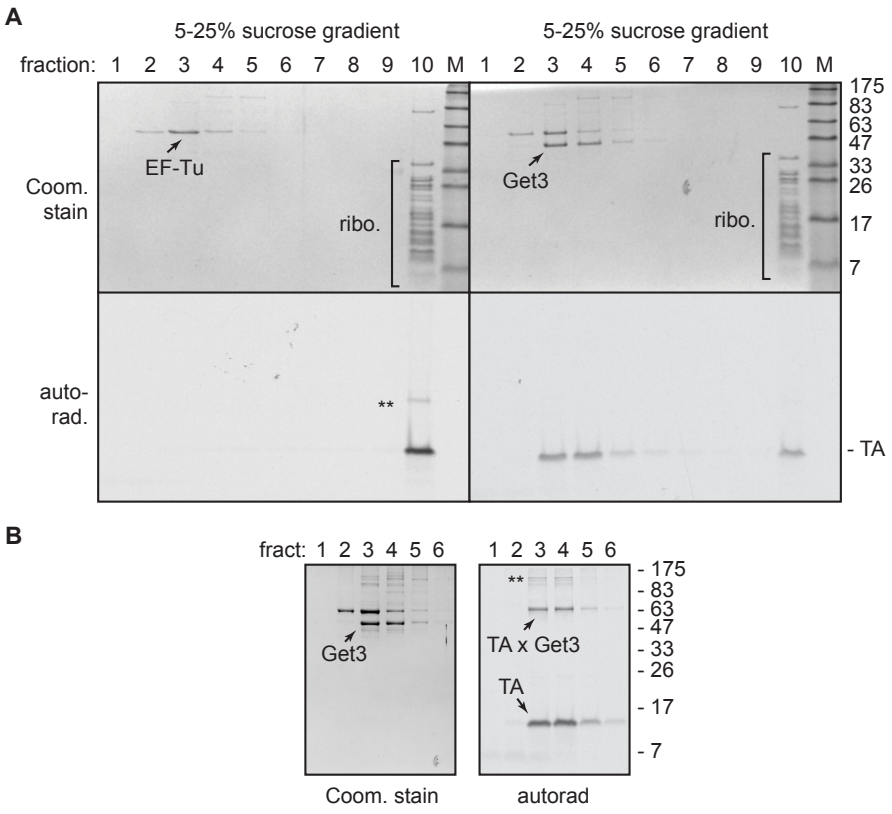

Fig. S3. Formation of Get3-TA complexes by *E. coli* PURE translation.

(A) TA protein was produced in the PURE translation system as in fig. S1 without and with 25 µM Get3. The reaction products were separated on a 5-25% sucrose gradient into 10 fractions and analyzed by SDS-PAGE, coomassie staining (top panels), and autoradiography (bottom panels). The ribosomes, which sediment to the bottom of the gradient, and EF-Tu (an abundant component of the PURE system visible by Coomassie staining) are indicated. The TA protein sediments to the bottom of the gradient (presumably as aggregates) in the absence of Get3 (left panel). This sample also contains some SDS-resistant dimers (asterisks) and higher order aggregates visible as a smear of increased molecular weight. Including Get3 in the reaction substantially reduces aggregation of the TA protein, which now co-migrates precisely with Get3 in fractions 3-5. **(B)** Fractions 1-6 from the gradients in panel A (right gel) were treated with the amine-reactive crosslinker DSS and analyzed by SDS-PAGE, coomassie staining, and autoradiography. The reaction containing Get3 results in a prominent new radiolabeled band representing the TA protein crosslinked to Get3 (TA x Get3). Minor species (asterisks) represent TA protein crosslinked to a crosslinked dimer of Get3.

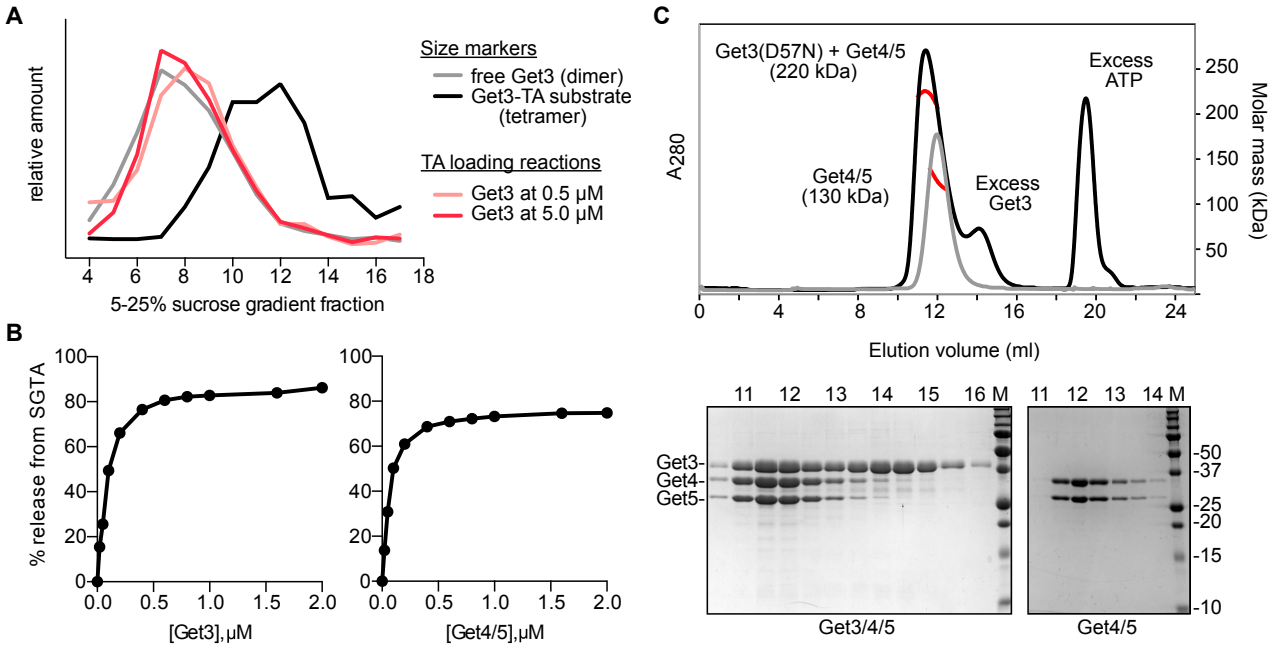

Fig. S4. Additional characterization of *in vitro* assembly reactions.

(A) A transfer reaction of TA protein from SGTA (0.5 µM) to Get3 via Get4-Get5 (0.5 µM) was conducted with either 0.5 µM Get3 or 5 µM Get3. The products of the reaction were then analyzed by 5-25% sucrose gradient in parallel with *E. coli* produced tetrameric Get3 complex and free dimeric Get3 for comparison. Regardless of Get3 concentration in the reaction, the Get3-TA protein complexes (red traces) co-migrate with free, dimeric Get3 (grey trace), not *E. coli* produced, tetrameric Get3 (black trace). Note that 5 µM Get3 is at least 5-fold higher than *in vivo* Get3 concentrations, and above the *K*d of 3.5 µM proposed for Get3 tetramerization (*22*). **(B)** Transfer reactions of TA protein from SGTA to Get3 were conducted in which either Get3 (left panel) or Get4-Get5 complex (right panel) was included at various concentrations ranging from 20 nM to 2 µM. The non-titrated components were kept constant at 0.5 µM, and the reaction allowed to proceed to completion (10 min; see fig. S2). The samples were then rapidly chilled, diluted in ice cold reaction buffer and analyzed for SGTA-TA crosslinks. The efficiency of release (quantified by phosphorimaging) is plotted. Note that both curves are hyperbolic in shape, without evidence for cooperativity. **(C)** SEC-MALLS traces for full-length Get4-Get5 (grey trace) and a Get3(D57N)-Get4-Get5 complex (black trace), obtained in the presence of 0.5 mM MgATP; the observed molecular mass of 220 kDa (red) for the Get3-Get4-Get5 complex corresponds to a single Get3 homodimer (experimentally verified mass 78.7 kDa) (*14*) bound to two copies of the Get4-Get5 heterodimer (expected mass for a 2:2:2 complex is 208.3 kDa). Peak fractions of the Get3-Get4-Get5 and Get4-Get5 complexes were analyzed by SDS-PAGE and Coomassie staining (bottom).

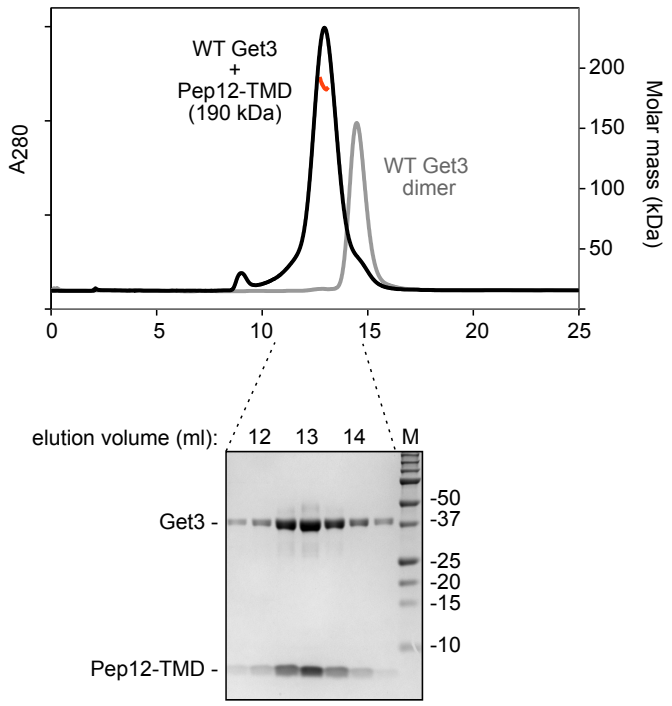

Fig. S5. Size analysis of *E. coli* produced wild-type Get3-TA substrate complex.

SEC-MALLS of wild-type Get3 bound to a truncated Pep12-TMD construct (4.6 kDa) produced by co-expression in *E. coli* (black). The observed molecular mass of 190 kDa (red) corresponds to a tetramer of Get3 (expected mass 157.4 kDa) complexed with 7.0 copies of TA substrate. A trace of dimeric Get3 (grey trace; experimentally verified mass 78.7 kDa) (*14*) is shown for comparison. Peak fractions of the tetrameric Get3 complex with Pep12-TMD were analyzed by SDS-PAGE and Coomassie staining (bottom).

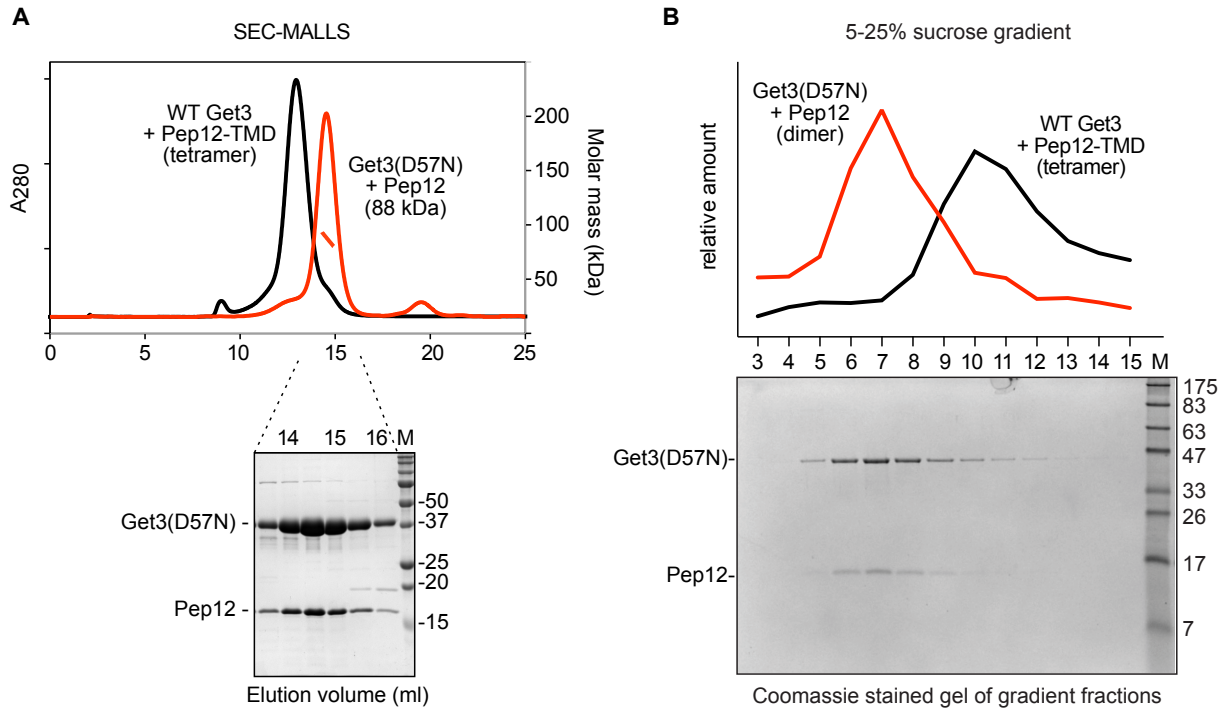

Fig. S6. Size analysis of *E. coli* produced Get3(D57N)-TA substrate complex.

(A) Get3(D57N) co-expressed with a modified TA substrate (StrepII-Sbh2-Pep12TMD-opsin;14.4 kDa) in *E. coli* was subjected to SEC-MALLS analysis (red). The observed molecular weight of 88 kDa corresponds to a dimer of Get3 (experimentally verified mass 78.7 kDa) (*14*) complexed with 0.63 copies of TA substrate. A trace of tetrameric WT Get3-Pep12-TMD complex (black; 190 kDa by MALLS; see fig. S5) is shown for comparison. Peak fractions of the dimeric Get3(D57N)-substrate complex were analyzed by SDS-PAGE and Coomassie staining (below). **(B)** Sucrose gradient analysis of the samples shown in panel A. The migration profile of the Get3(D57N)-TA substrate complex is plotted (red); the tetrameric complex is shown for comparison (black). Coomassie stained gel of the Get3(D57N)-TA substrate fractions is shown below the graph. Note that the Get3(D57N)-substrate complex migrates precisely where physiologically loaded (*i.e.*, via Get4-Get5) Get3-TA substrate complexes migrate on these gradients (compare to Fig. 1E).

A

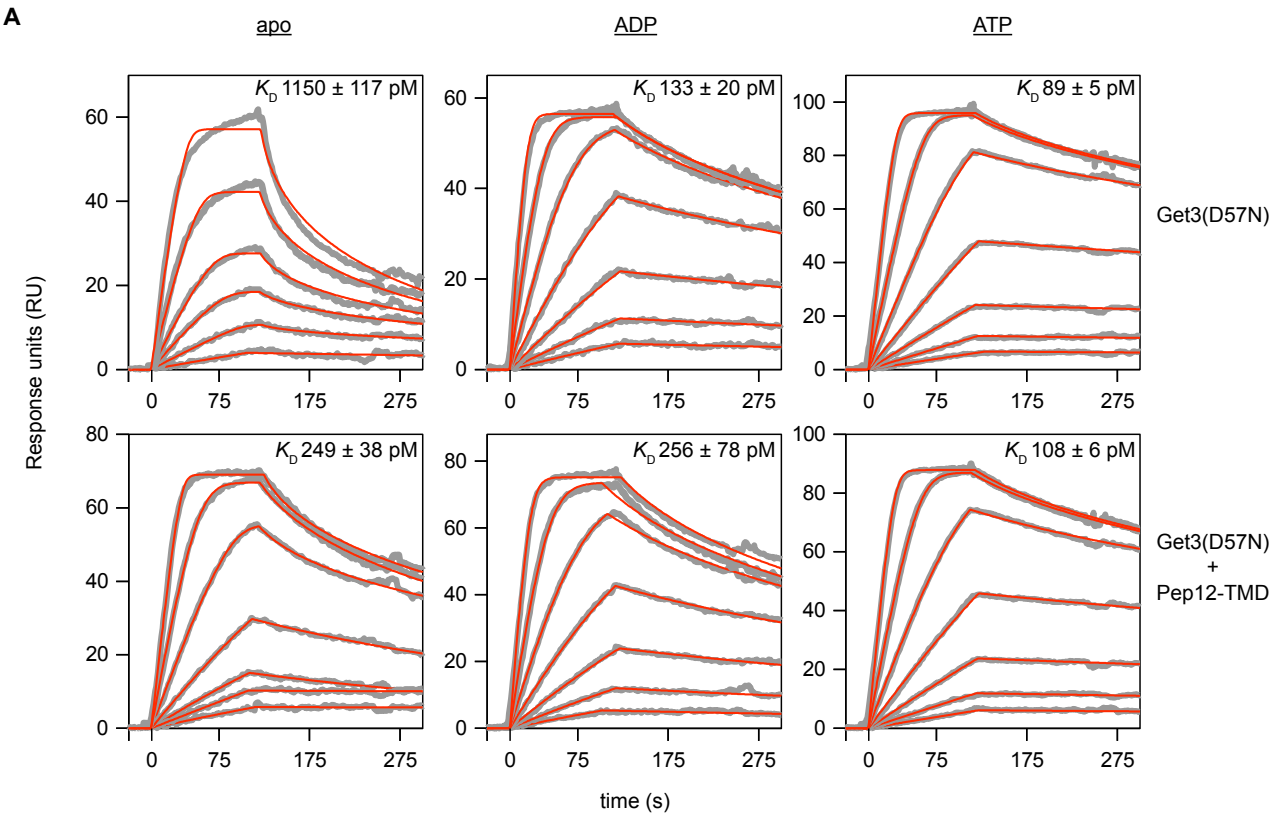

B

Construct	Condition	k_a (x 10^7 M^{-1} s^{-1})	k_d (x 10^{-3} s^{-1})	K_D (pM)
Get3(D57N)	Apo	6.2 ± 0.7	73 ± 13	1150 ± 117
	MgADP	2.2 ± 0.5	2.9 ± 0.3	133 ± 20
	MgATP	2.4 ± 0.2	2.1 ± 0.09	89 ± 5
Get3(D57N) + Pep12-TMD	Apo	2.6 ± 0.6	6.3 ± 0.6	249 ± 38
	MgADP	1.8 ± 0.6	4.2 ± 0.5	256 ± 78
	MgATP	2.3 ± 0.1	2.5 ± 0.03	108 ± 6

Fig. S7. Kinetic analysis of sAB binding.

(A) SPR sensorgrams (grey) were obtained for three different nucleotide states (apo, MgADP and MgATP) with either free Get3(D57N), or Get3(D57N) bound to Pep12-TMD. For the free Get3 measurements, Get3(D57N) was immobilized on an NTA sensor chip via its N-terminal 6xHis tag. For the targeting complex measurements, the complex was immobilized via an N-terminal 6xHis tag on the TA substrate to ensure that the observed responses were due to sAB binding to the targeting complex instead of free Get3. For determination of kinetic rate constants, datasets were fit to a simple 1:1 interaction model using nonlinear regression analysis (red). **(B)** Summary table of the extracted rates and binding constants. Mean +/- s.d. (n=3) are shown.

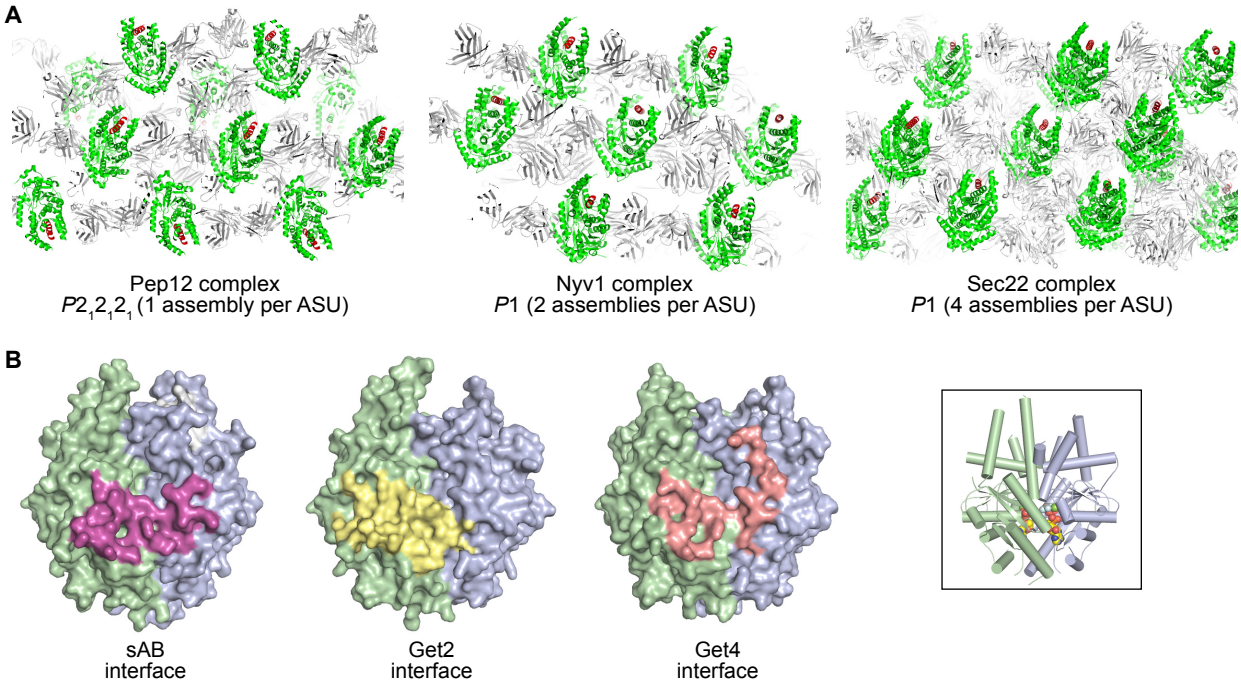

Fig. S8. Protein-protein interactions in the crystallized complexes.

(A) Comparison of the packing arrangements in the three different Get3-TA-sAB structures; Get3 (green), TMD (red), and sAB (grey) are indicated. Get3 dimers, but not higher-order oligomers, are observed in three different crystal forms. In each case, the majority of contacts are mediated by sAB-sAB and sAB-Get3 interactions. **(B)** The crystallization sAB binds to an interaction 'hot-spot' (magenta) at the Get3 closed dimer interface (green, blue). The corresponding interaction surfaces are shown for the Get2 (yellow) and Get4 (salmon). Inset shows the orientation of the Get3 dimer and location of bound nucleotide.

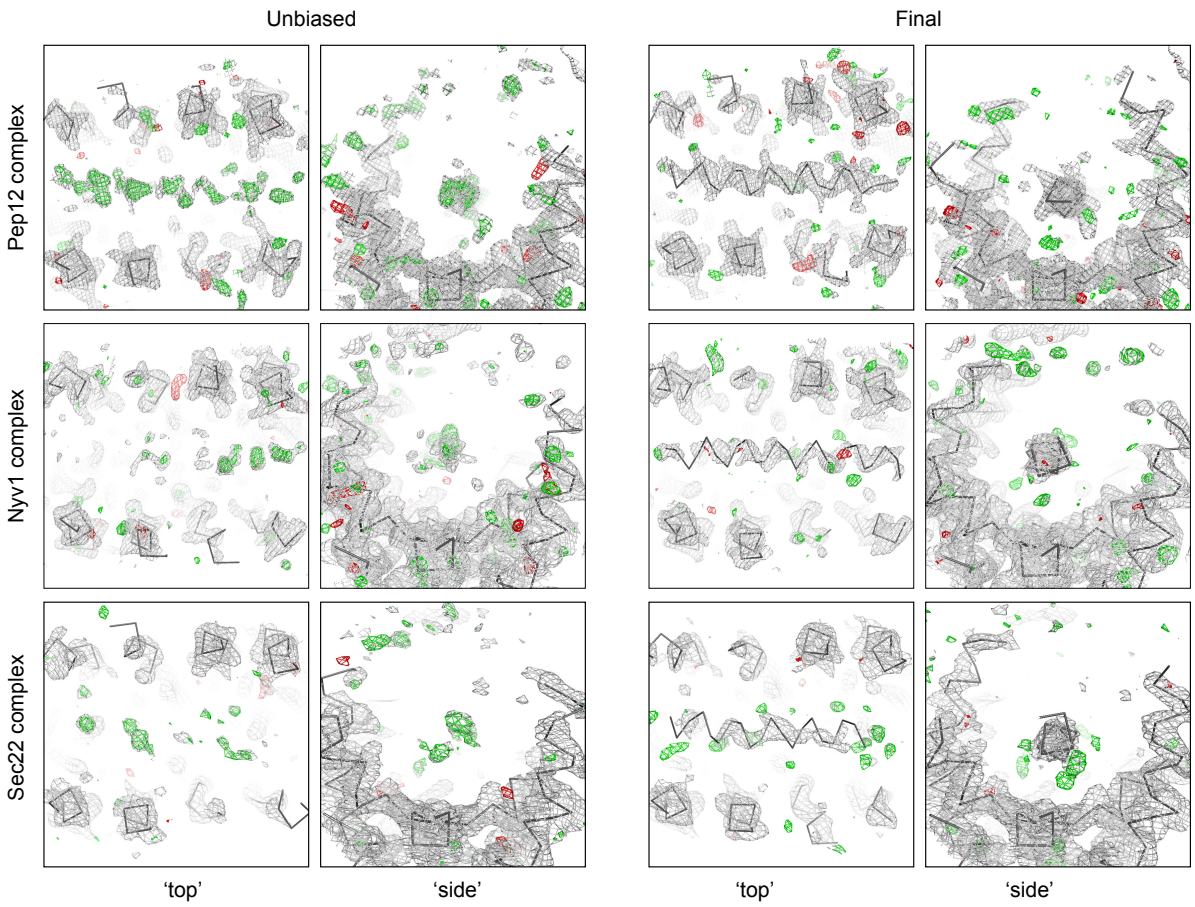

Fig. S9. Electron density maps for the *S. cerevisiae* Get3(D57N)-TMD complexes.

'Top' and 'side' views looking into the hydrophobic groove. Electron density is from σA-weighted 2*F*o-*F*c (grey) and *F*o-*F*c (green, red) maps calculated at 2.05 Å (Pep12), 2.35 Å (Nyv1) and 2.75 Å (Sec22) resolution and contoured at 1.0σ (Pep12) or 0.9σ (Nyv1 and Sec22) and +/- 3.0σ. Unbiased maps were generated at an early stage of the refinement prior to addition of the TMD and waters to the model (grey ribbon). Final maps were calculated with phases from the fully refined model. Despite relatively weak density (likely due to flexibility, partial occupancy and/or statistical disorder), the unbiased Pep12 maps reveal a helical TMD substrate within the groove (note the periodicity of the difference density). Density for the Nyv1 and Sec22 TMDs was weaker, but note the positive *F*o-*F*c (green) density along the helical axis (most easily visible in the 'side' views), and the absence of negative *F*o-*F*c (red) density. Thus, we modeled the Nyv1 and Sec22 TMDs as poly-alanine helices, and did not assign sequence or orientation.

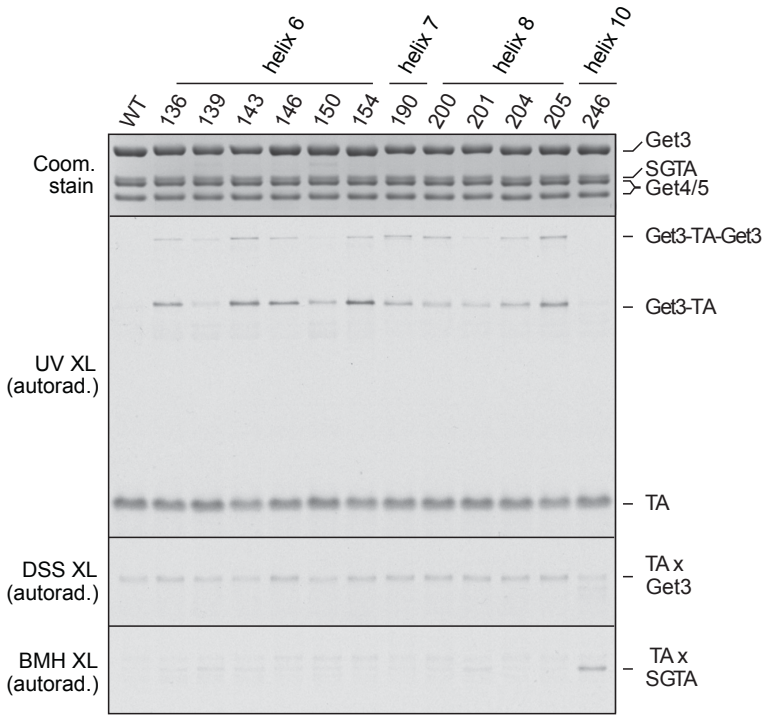

Fig. S10. Site-specific photocrosslinking analysis of TA substrate binding.

SGTA-TA substrate complexes were prepared and subjected to transfer reactions exactly as in Fig. 1C. The Get3 protein in the reaction was either wild-type or contained a benzophenone at the indicated position. Immediately following the transfer reaction, samples were divided and subjected to UV crosslinking (via the benzophenone), DSS crosslinking to detect Get3-TA interactions and BMH crosslinking to detect SGTA-TA interactions. Note that all Get3 proteins induce release of TA protein from SGTA and capture substrate except 246, whose interaction with Get4 is impaired. The uncrosslinked TA protein and its adducts to the indicated partners are indicated. An aliquot of the sample was also analyzed by coomassie staining to visualize the input proteins.

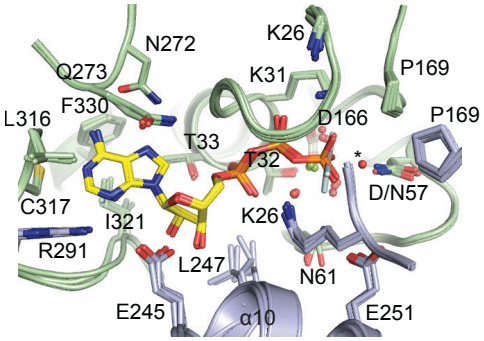

Fig. S11. Comparison of active site geometry in free and TMD-bound Get3.

Active sites from the Pep12 (ADP/ATP), Nyv1 (ATP) and Sec22 (ADP/ATP) targeting complexes are superimposed on the active site of free Get3 (ADP-AlF_4^-) (2woj). The active site conformation is nearly identical in all cases, with essential residues, including K26 and D57 (Asn in the mutants), organized for hydrolysis. A portion of the loosely conserved A-loop region (including Gly319 and Glu320) as well as Arg322 and Phe246 (which form part of the sAB-Get3 interface) undergo slight shifts in the sAB-targeting complexes. The asterisk marks the putative nucleophilic water coordinated by D57 in the free Get3-ADP-AlF_4^- structure.

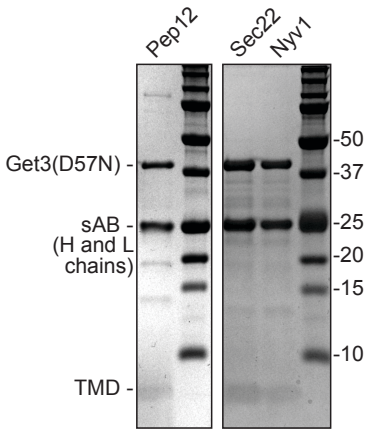

Fig. S12. Composition of the Get3-TMD-sAB complex crystals.

Multiple crystals from drops containing Get3(D57N)-TA complexes with sAB were washed by 5x serial transfer through stabilizing buffer, dissolved in SDS-PAGE loading buffer (containing fresh β-mercaptoethanol), separated on 12% Tris-tricine gels, and visualized by Coomassie staining. Note that the ~25 kDa band corresponds to overlapping heavy (H) and light (L) chains of the crystallization sAB. The small (4.6 kDa), hydrophobic TMD is visible as a faint band at the bottom of the gel.

Table S1. Data collection and refinement statistics

	Pep12	Nyv1	Sec22
Data collection			
Space group	$P2_12_12_1$	$P1$	$P1$
Cell dimensions			
a, *b*, *c* (Å)	102.9, 112.0, 153.7	79.4, 109.2, 111.4	112.6, 119.5, 147.6
α, β, γ (°)	90.0, 90.0, 90.0	63.1 77.7 70.2	71.9, 89.9, 66.6
Wavelength (Å)	0.9795	0.9795	0.9795
Resolution (Å)	53.95-2.05 (2.12-2.05)*	69.38-2.35 (2.43-2.35)	39.72 -2.75 (2.85-2.75)
Redundancy	3.8 (3.6)	3.2 (3.0)	1.7 (1.7)
Completeness (%)	98 (90)	95 (85)	91 (89)
$I/\sigma I$	11.7 (2.1)	5.9 (1.8)	8.2 (1.4)
R_{meas} (%)	7.2 (63.8)	14.1 (49.4)	9.0 (70.2)
$CC_{1/2}$ (%)	99.8 (76.7)	98.8 (82.3)	99.7 (62.8)
Refinement			
Resolution range (Å)	53.95-2.05	69.38-2.35	39.72 -2.75
No. Reflections	109335	123349	157053
R_{work}/R_{free} (%)	18.3/21.8	19.2/23.4	19.6/24.8
No. of non-H atoms			
Protein	11682	23007	45806
Ligands	119	130	476
Solvent	928	808	425
Average B ($Å^2$)			
Protein	52.3	61.8	75.9
Ligands	38.7	39.9	46.3
Solvent	51.4	49.0	50.6
R.M.S. Deviations			
Bond lengths (Å)	0.007	0.005	0.008
Bond angles (°)	1.0	0.95	0.99
Ramachandran analysis			
Favored (%)	97.6	97.1	96.8
Allowed (%)	2.1	2.7	2.7
Outliers (%)	0.27	0.17	0.43

Each dataset was obtained from a single crystal.
*Values in parentheses refer to the high-resolution shell.

References and Notes

1. D. Akopian, K. Shen, X. Zhang, S. O. Shan, Signal recognition particle: An essential protein-targeting machine. *Annu. Rev. Biochem.* **82**, 693–721 (2013). Medline doi:10.1146/annurev-biochem-072711-164732

2. J. W. Chartron, W. M. Clemons Jr., C. J. Suloway, The complex process of GETting tail-anchored membrane proteins to the ER. *Curr. Opin. Struct. Biol.* **22**, 217–224 (2012). Medline doi:10.1016/j.sbi.2012.03.001

3. V. Denic, V. Dötsch, I. Sinning, Endoplasmic reticulum targeting and insertion of tail-anchored membrane proteins by the GET pathway. *Cold Spring Harb. Perspect. Biol.* **5**, a013334 (2013). Medline doi:10.1101/cshperspect.a013334

4. R. S. Hegde, R. J. Keenan, Tail-anchored membrane protein insertion into the endoplasmic reticulum. *Nat. Rev. Mol. Cell Biol.* **12**, 787–798 (2011). Medline doi:10.1038/nrm3226

5. V. Favaloro, M. Spasic, B. Schwappach, B. Dobberstein, Distinct targeting pathways for the membrane insertion of tail-anchored (TA) proteins. *J. Cell Sci.* **121**, 1832–1840 (2008). Medline doi:10.1242/jcs.020321

6. M. Schuldiner, J. Metz, V. Schmid, V. Denic, M. Rakwalska, H. D. Schmitt, B. Schwappach, J. S. Weissman, The GET complex mediates insertion of tail-anchored proteins into the ER membrane. *Cell* **134**, 634–645 (2008). Medline doi:10.1016/j.cell.2008.06.025

7. S. Stefanovic, R. S. Hegde, Identification of a targeting factor for posttranslational membrane protein insertion into the ER. *Cell* **128**, 1147–1159 (2007). Medline doi:10.1016/j.cell.2007.01.036

8. G. Bozkurt, G. Stjepanovic, F. Vilardi, S. Amlacher, K. Wild, G. Bange, V. Favaloro, K. Rippe, E. Hurt, B. Dobberstein, I. Sinning, Structural insights into tail-anchored protein binding and membrane insertion by Get3. *Proc. Natl. Acad. Sci. U.S.A.* **106**, 21131–21136 (2009). Medline doi:10.1073/pnas.0910223106

9. J. Hu, J. Li, X. Qian, V. Denic, B. Sha, The crystal structures of yeast Get3 suggest a mechanism for tail-anchored protein membrane insertion. *PLOS ONE* **4**, e8061 (2009). Medline doi:10.1371/journal.pone.0008061

10. A. Mateja, A. Szlachcic, M. E. Downing, M. Dobosz, M. Mariappan, R. S. Hegde, R. J. Keenan, The structural basis of tail-anchored membrane protein recognition by Get3. *Nature* **461**, 361–366 (2009). Medline doi:10.1038/nature08319

11. C. J. Suloway, J. W. Chartron, M. Zaslaver, W. M. Clemons Jr., Model for eukaryotic tail-anchored protein binding based on the structure of Get3. *Proc. Natl. Acad. Sci. U.S.A.* **106**, 14849–14854 (2009). Medline doi:10.1073/pnas.0907522106

12. A. Yamagata, H. Mimura, Y. Sato, M. Yamashita, A. Yoshikawa, S. Fukai, Structural insight into the membrane insertion of tail-anchored proteins by Get3. *Genes Cells* **15**, 29–41 (2010). Medline doi:10.1111/j.1365-2443.2009.01362.x

13. S. Stefer, S. Reitz, F. Wang, K. Wild, Y. Y. Pang, D. Schwarz, J. Bomke, C. Hein, F. Löhr, F. Bernhard, V. Denic, V. Dötsch, I. Sinning, Structural basis for tail-anchored membrane protein biogenesis by the Get3-receptor complex. *Science* **333**, 758–762 (2011). Medline

14. M. Mariappan, A. Mateja, M. Dobosz, E. Bove, R. S. Hegde, R. J. Keenan, The mechanism of membrane-associated steps in tail-anchored protein insertion. *Nature* **477**, 61–66 (2011). Medline doi:10.1038/nature10362

15. F. Wang, C. Chan, N. R. Weir, V. Denic, The Get1/2 transmembrane complex is an endoplasmic-reticulum membrane protein insertase. *Nature* **512**, 441–444 (2014). Medline doi:10.1038/nature13471

16. F. Wang, A. Whynot, M. Tung, V. Denic, The mechanism of tail-anchored protein insertion into the ER membrane. *Mol. Cell* **43**, 738–750 (2011). Medline doi:10.1016/j.molcel.2011.07.020

17. F. Wang, E. C. Brown, G. Mak, J. Zhuang, V. Denic, A chaperone cascade sorts proteins for posttranslational membrane insertion into the endoplasmic reticulum. *Mol. Cell* **40**, 159–171 (2010). Medline doi:10.1016/j.molcel.2010.08.038

18. M. Mariappan, X. Li, S. Stefanovic, A. Sharma, A. Mateja, R. J. Keenan, R. S. Hegde, A ribosome-associating factor chaperones tail-anchored membrane proteins. *Nature* **466**, 1120–1124 (2010). Medline doi:10.1038/nature09296

19. J. W. Chartron, C. J. Suloway, M. Zaslaver, W. M. Clemons Jr., Structural characterization of the Get4/Get5 complex and its interaction with Get3. *Proc. Natl. Acad. Sci. U.S.A.* **107**, 12127–12132 (2010). Medline doi:10.1073/pnas.1006036107

20. H. B. Gristick, M. Rao, J. W. Chartron, M. E. Rome, S. O. Shan, W. M. Clemons Jr., Crystal structure of ATP-bound Get3-Get4-Get5 complex reveals regulation of Get3 by Get4. *Nat. Struct. Mol. Biol.* **21**, 437–442 (2014). Medline doi:10.1038/nsmb.2813

21. M. E. Rome, U. S. Chio, M. Rao, H. Gristick, S. O. Shan, Differential gradients of interaction affinities drive efficient targeting and recycling in the GET pathway. *Proc. Natl. Acad. Sci. U.S.A.* **111**, E4929–E4935 (2014). Medline doi:10.1073/pnas.1411284111

22. M. E. Rome, M. Rao, W. M. Clemons, S. O. Shan, Precise timing of ATPase activation drives targeting of tail-anchored proteins. *Proc. Natl. Acad. Sci. U.S.A.* **110**, 7666–7671 (2013). Medline doi:10.1073/pnas.1222054110

23. C. J. Suloway, M. E. Rome, W. M. Clemons Jr., Tail-anchor targeting by a Get3 tetramer: The structure of an archaeal homologue. *EMBO J.* **31**, 707–719 (2012). Medline doi:10.1038/emboj.2011.433

24. J. W. Chartron, D. G. VanderVelde, W. M. Clemons Jr., Structures of the Sgt2/SGTA dimerization domain with the Get5/UBL4A UBL domain reveal an interaction that forms a conserved dynamic interface. *Cell Reports* **2**, 1620–1632 (2012). Medline doi:10.1016/j.celrep.2012.10.010

25. M. Paduch, A. Koide, S. Uysal, S. S. Rizk, S. Koide, A. A. Kossiakoff, Generating conformation-specific synthetic antibodies to trap proteins in selected functional states. *Methods* **60**, 3–14 (2013). Medline doi:10.1016/j.ymeth.2012.12.010

26. T. Hainzl, S. Huang, G. Meriläinen, K. Brännström, A. E. Sauer-Eriksson, Structural basis of signal-sequence recognition by the signal recognition particle. *Nat. Struct. Mol. Biol.* **18**, 389–391 (2011). Medline doi:10.1038/nsmb.1994

27. C. Y. Janda, J. Li, C. Oubridge, H. Hernández, C. V. Robinson, K. Nagai, Recognition of a signal peptide by the signal recognition particle. *Nature* **465**, 507–510 (2010). Medline doi:10.1038/nature08870

28. W. Voth, M. Schick, S. Gates, S. Li, F. Vilardi, I. Gostimskaya, D. R. Southworth, B. Schwappach, U. Jakob, The protein targeting factor Get3 functions as ATP-independent chaperone under oxidative stress conditions. *Mol. Cell* **56**, 116–127 (2014). Medline doi:10.1016/j.molcel.2014.08.017

29. R. J. Keenan, D. M. Freymann, P. Walter, R. M. Stroud, Crystal structure of the signal sequence binding subunit of the signal recognition particle. *Cell* **94**, 181–191 (1998). Medline doi:10.1016/S0092-8674(00)81418-X

30. J. W. Chin, A. B. Martin, D. S. King, L. Wang, P. G. Schultz, Addition of a photocrosslinking amino acid to the genetic code of Escherichiacoli. *Proc. Natl. Acad. Sci. U.S.A.* **99**, 11020–11024 (2002). Medline doi:10.1073/pnas.172226299

31. G. Winter, *xia2* : An expert system for macromolecular crystallography data reduction. *J. Appl. Cryst.* **43**, 186–190 (2010). doi:10.1107/S0021889809045701

32. W. Kabsch, XDS. *Acta Crystallogr. D Biol. Crystallogr.* **66**, 125–132 (2010). Medline doi:10.1107/S0907444909047337

33. A. J. McCoy, R. W. Grosse-Kunstleve, P. D. Adams, M. D. Winn, L. C. Storoni, R. J. Read, *Phaser* crystallographic software. *J. Appl. Cryst.* **40**, 658–674 (2007). doi:10.1107/S0021889807021206

34. S. S. Rizk, M. Paduch, J. H. Heithaus, E. M. Duguid, A. Sandstrom, A. A. Kossiakoff, Allosteric control of ligand-binding affinity using engineered conformation-specific effector proteins. *Nat. Struct. Mol. Biol.* **18**, 437–442 (2011). Medline doi:10.1038/nsmb.2002

35. P. D. Adams, P. V. Afonine, G. Bunkóczi, V. B. Chen, I. W. Davis, N. Echols, J. J. Headd, L. W. Hung, G. J. Kapral, R. W. Grosse-Kunstleve, A. J. McCoy, N. W. Moriarty, R. Oeffner, R. J. Read, D. C. Richardson, J. S. Richardson, T. C. Terwilliger, P. H. Zwart, PHENIX: A comprehensive Python-based system for macromolecular structure solution. *Acta Crystallogr. D Biol. Crystallogr.* **66**, 213–221 (2010). Medline doi:10.1107/S0907444909052925

36. P. Emsley, B. Lohkamp, W. G. Scott, K. Cowtan, Features and development of Coot. *Acta Crystallogr. D Biol. Crystallogr.* **66**, 486–501 (2010). Medline doi:10.1107/S0907444910007493

37. E. Pedrazzini, A. Villa, R. Longhi, A. Bulbarelli, N. Borgese, Mechanism of residence of cytochrome b(5), a tail-anchored protein, in the endoplasmic reticulum. *J. Cell Biol.* **148**, 899–914 (2000). Medline doi:10.1083/jcb.148.5.899